Aluminum combustion in CO2-CO-N2 mixtures

Alexandre Braconnier, Stany Gallier, Fabien Halter, Christian Chauveau

Aluminum combustion in CO_2-CO-N_2 mixtures

Alexandre BRACONNIER[a,b], Stany GALLIER[a,*], Fabien HALTER[b], Christian CHAUVEAU[b]

[a] *ArianeGroup, Le Bouchet Research Center, 91710 Vert-le-Petit, France*
[b] *CNRS-ICARE, University of Orléans, 45000 Orléans, France*

Abstract

This paper considers a new experimental set-up to image and study the combustion of a single burning aluminum droplet, which is levitated electrostatically. This work focuses on CO_2, CO and mixtures thereof, that have not or scarcely been studied. Aluminum is found to burn in pure CO_2 in a diffusion mode (with a $D_0^{1.9}$ scaling, where D_0 is the initial particle diameter) whereas combustion in pure CO is kinetically limited and halts swiftly, irrespective of pressure in the range 1–15 atm. Mixtures of CO_2 and CO suggest a major driving effect from CO_2 compared to CO. Overall, CO and N_2 behave as inert species. All the burning time data are processed to propose a new empirical correlation for CO_2-CO-N_2 mixtures that significantly improves the widely used Beckstead's correlation while including the role of CO and N_2.

Keywords: Aluminum combustion, Burning time correlation, Solid propulsion

*Corresponding author: stany.gallier@ariane.group

1. Introduction

Aluminum is widely used as an energetic additive in solid propellants to increase performance. It has also received a growing interest in aviation fuels [1], as a source of hydrogen for fuel cell applications [2], or in novel power generation concepts [3, 4] as it provides a carbon-free energy that meets current trends for reducing emissions of greenhouse gases.

However aluminum combustion is complex and, despite decades of fundamental studies, is not completely understood so far. It is generally accepted that large particles (i.e. $\gtrsim$ 10-20 μm) are expected to burn in the vapor-phase through a diffusion flame. The burning time t_b of a particle is a major sizing parameter for practical applications. For instance, in solid rocket motors, this burning time is of high importance since it controls the occurrence of incomplete combustion (if burning time is longer than residence time in the chamber) or the onset of thermoacoustic instabilities [5]. By compiling available experimental data, Beckstead et al. [6] proposed the following widely used correlation for the burning time t_b of a droplet of initial diameter D_0

$$t_b = \frac{0.00735 D_0^{1.8}}{p^{0.1} T^{0.2} (X_{O_2} + 0.6 X_{H_2O} + 0.22 X_{CO_2})} \qquad (1)$$

with X the mole fraction and units: atm-K-μm-ms. This relation suggests a combustion driven by droplet vaporization and following an (almost) D^2 law, with limited effects of pressure p and temperature T. This is fairly consistent with a diffusion-limited combustion. This correlation also indicates the relative effects of oxidizers, with a larger oxidizing efficiency for O_2 compared to H_2O and CO_2.

Major oxidizers released in combustion systems (e.g. solid propellants) are CO_2, CO, and H_2O. Yet, most experimental data are obtained in O_2 mixtures at atmospheric pressures. This strongly differs from real systems and there is a strong need to acquire data for more relevant conditions, especially for the less documented species. We can therefore anticipate that Eq. (1) is accurate for O_2 mixtures—which was already confirmed in our previous experiments [7]—but its adequacy in CO_2- or CO-rich atmosphere needs to be further assessed. Indeed it was noted by Gill et al. [8] that this correlation could be hardly extrapolated to conditions different from those used to establish it. Moreover, the lack of any dependency on CO or N_2 fraction in Eq. (1) also requires further experimental confirmation, which will be part of this study. Note that we here only address CO_2 and CO while the study of H_2O is deferred to future studies.

Experimental data in CO_2 remain relatively limited with most significant contributions provided in Ref. [8–13]. Data suggest that CO_2 has a lower oxidizing efficiency compared to O_2, thereby giving longer burning times. Servaites et al. [12] noted a non-linear relationship as a function of concentration in CO_2/O_2 mixtures. Combustion of large particles was characterized by a diffusion flame regime with moderate flame temperatures ($\sim$ 3300 K) and the presence of non-stoichiometric oxycarbide phases was detected on quenched particles [10]. Combustion time measurements in pure CO_2 are extremely limited and were provided only by very few authors [10, 13, 14].

Experimental data in CO are even scarcer and studies in pure CO have only been provided in the works of Bucher et al. [9]. They reported no diffusion flames and species distributions suggested that heterogeneous reactions can take place on the droplet surface, generating complex condensed-phase products on the surface with Al_2O_3 and carbon-containing compounds. Note that there are other few experiments including CO from tests involving propellants [15] or gaseous flames [16] but CO was present in limited quantity and its role not specifically studied.

In the present paper, we provide new results in CO_2 and CO atmospheres with a dedicated experimental set-up. A novelty of this work relies on considering different CO_2-CO mixtures, that are conditions for which no data is available although this is a common combination of combustion gas in solid rockets. A final outcome of this study is a new experimental correlation expected to be more reliable for O_2-CO_2-CO-N_2 atmospheres.

2. Experimental set-up

A new, dedicated set-up has been developed to study the combustion mechanism of a burning aluminum particle under high pressure conditions. It consists of an electrodynamic levitator in which a single particle, levitated by electrostatic forces, burns in a controlled atmosphere. This approach is non-intrusive—without any contacting support with the particle—and involves no flow/convective effects, unlike free-fall set-ups or aerodynamic levitators. Another advantage is that the atmosphere in which the particle burns is precisely controlled and offers a large spectrum of pressure (1$\sim$120 atm) and nature of gases. It has been already described extensively in [17] and is here only briefly recalled. Note that this is basically the set-up used by Legrand et al. [13] although in an improved version, notably with the use of high-speed video.

As depicted in Fig. 1, the levitator is composed of

electrodes supplied by AC and DC voltages which allow setting the horizontal and vertical position of an aluminum particle that has been tribo-charged beforehand. This levitator is located in a high-pressure chamber with adjustable gas atmospheres. A CO_2 laser beam is used to irradiate and ignite the aluminum particle. We have conducted different tests confirming negligible effects—if any—of the electric field on the combustion process. In particular, any deformation of the flame along the electric field has never been noticed. Diagnostics mainly consist of optical measurements including two photomultiplier tubes (PM) and a high-speed camera (Phantom V1611) combined with a long-distance microscope (Questar QM100). This allows for a high temporal and spatial resolution (up to 40000 fps and 2.5 μm/px). For clarity, Fig. 1 depicts only one PM: the second PM is located nearby and oriented at 90^o ; both receive the same signal from a beamsplitter cube. Two PMs are used for redundancy reasons ; their wavelengths (at 488 nm and 514 nm, respectively) lie in the spectrum of AlO emission. The laser is synchronized with photomultipliers and is shut down as the particle is ignited to ensure a self-sustained, and not laser-assisted, combustion.

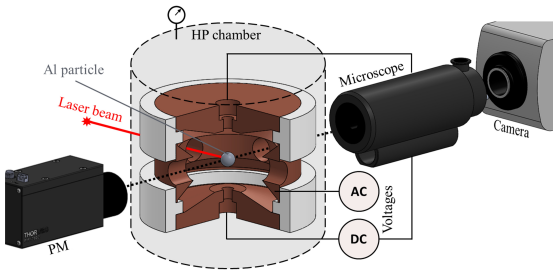

Figure 1: Schematic representation of the electrodynamic levitator

As already mentioned, the combustion time t_b is the main quantity of interest and, in this study, is estimated based on photomultiplier signals, i.e. direct light emission. A novelty of our set-up however is that automatic image processing can also provide time-resolved evolution of particle diameter $D(t)$. Interestingly, this allows computing the evaporation rate $K=dD^2/dt$, which is the major input data for classical D^2 models. Note that if a D^2 law holds, then K is constant and $t_b=D_0^2/K$. Figure 2 illustrates a typical particle diameter regression as obtained with our set-up and previously published [18]. The initial diameter (here, D_0=66 μm) is measured from image processing right before ignition (prescribed at t=0) after particle melting. Transient flame development right after ignition may temporarily hinder an accurate tracking of particle, which explains the loss of information in the initial combustion phase. As seen from Fig. 2, it is possible to track the particle evolution during a significant part of the combustion. A black line corresponding to a D^2 regression has been added and it fits the experimental evolution fairly well . Unfortunately, particle detection until complete burning is difficult, which explains a premature termination of data for lowest diameters. This arises mostly due to large oxide lobe developing on particle surface, or particle moving out of the focal plane, or even particle hidden by luminous flame at highest pressures. All those difficulties in particle tracking explain why direct visualization is complemented by PM. However detailed information on the burning process in the early phase of combustion allows for a new—and scarcely reported—information that complements a global burning time. This will be made clearer in the next section. Therefore, both burning times t_b (obtained using PM) and evaporation constant K (by direct imaging) are presented throughout the paper.

Experimental conditions consider different gas mixtures including CO_2, CO, N_2 and O_2. Pressures investigated span between 1 and 15 atm. Gas is not preheated and is at room temperature ($\approx$ 293 K). Aluminum particles are sourced from Hermillon company, France. Diameters are in the range 30–130 μm, typical of solid rocket applications and presumably burning in the diffusion regime.

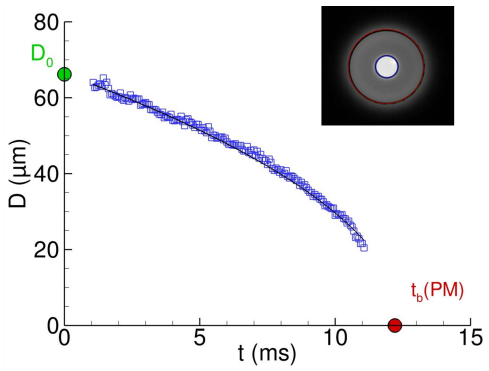

Figure 2: Typical diameter evolution $D(t)$ obtained from direct imaging (D_0=66 μm, air, p=6 atm) from [18]. Particle ignition is set at t=0. Red circle indicates the burning time t_b measured by PM. Solid black line corresponds to a D^2 regression. Inset: example of image processing showing detection of particle (blue circle) and flame (red circle).

3. Results

3.1. Pure CO_2

The combustion sequence of a D_0=88 μm particle burning in pure CO_2 at ambient pressure is illustrated in Fig. 3. The initial irregular shape of the particle turns spherical after melting. Right after ignition, an envelope flame is visible supporting a diffusion-limited combustion. The bright oxide lobe on the particle is clearly visible throughout the combustion making the flame asymmetric as the lobe grows (final picture). The behavior is qualitatively similar at higher pressures although the flame is brighter and oxide lobe grows faster. Qualitative considerations on combustion mechanisms are not addressed in further detail here and may be found in a previous paper [19].

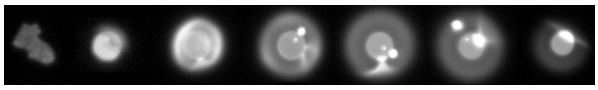

Figure 3: Typical combustion sequence in pure CO_2 (p=1 atm, D_0=88 μm.)

Figure 4 compiles experimental burning times—obtained from photomultiplier signals—for different pressures p=1, 5, and 10 atm (other data are also obtained at 8 and 15 atm but not displayed here for clarity) and initial diameters D_0. In the figure are also presented data at 1 atm from literature [10, 13] as well as Beckstead's correlation Eq. (1) in solid lines for the three pressures. Our experimental data are globally in line with reported data although slightly longer burning times are measured. Note that we choose here to display data using natural scale instead of logarithmic scale so as to make differences clearer. Measured burning times are lower than predicted by Beckstead's correlation, 20 % less on average. We believe this can be explained by the limited number of data on CO_2 mixtures (and none in pure CO_2) used to set the correlation. As expected from diffusion-limited combustion, burning times t_b roughly follow a D^2 law. More specifically, fitting a D^n law pressure-by-pressure, gives an average exponent n=1.90 ± 0.08. Burning times are weakly affected by pressure with faster combustion at higher pressures. A $D^n p^\alpha$ fit on all our results in pure CO_2 (i.e., 90 data points) yields α=−0.10 which is exactly the value found by Beckstead, although the exact agreement might be fortuitous.

As discussed in Sec. 2, an alternative way to present results is by plotting the evaporation rate K=dD^2/dt, which is size-independent if a D^2 law holds. Image analysis, however, supports that K is indeed a constant

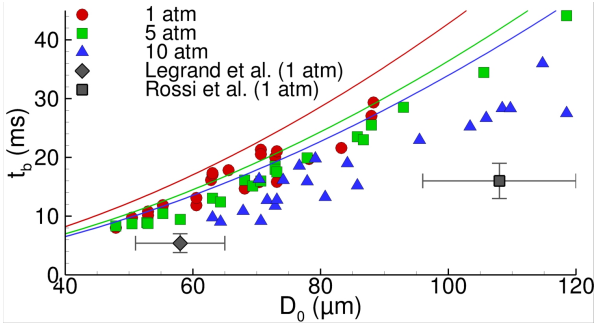

Figure 4: Measured burning time t_b with particle size D_0 and pressure as well as data from literature [10, 13]. Lines: Beckstead's correlation Eq. (1).

at a given pressure, or said differently, a quasi-D^2 behavior is found at the beginning of combustion—similarly to results from Fig. 2. Unlike previous burning times, we recall that evaporation rate is here directly measured from image processing during early combustion. Figure 5 presents the evaporation constant K as well as a $p^{0.1}$ evolution, which would be expected for a burning time scaling as $p^{-0.1}$, as attested by present results or Beckstead's data (recalling that K=D_0^2/t_b). It seems that K is almost pressure-independent and does not follow this $p^{0.1}$ scaling. By and large, this means that the beginning of combustion (measured by K) does fit theoretical expectations—with a D^2 scaling and absence of pressure effect—while overall burning time not (slightly lower exponent n and pressure effect).

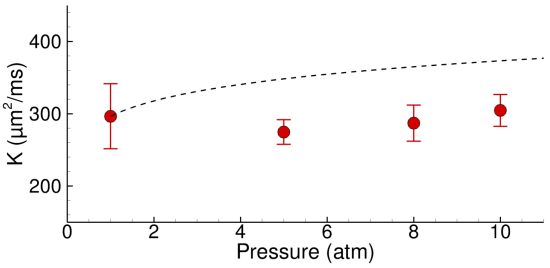

Figure 5: Evaporation constant K from direct imaging. Dashed line: $p^{0.1}$ dependence that would be expected from burning time measurements.

Deviation from classical D^2 behavior is therefore believed to occur mostly at the latest stages of combustion. This can for instance arise from massive oxide lobe formation on particle surface (which reduces the available surface for evaporation), kinetically controlled combustion at smallest size, or incomplete combustion (e.g. due to violent fragmentation at end of the burning). This is where K is worth considering, especially regard-

ing model validation: K is related to early combustion stage where a D^2 law still holds while t_b is more global and incorporates many poorly understood effects occurring at combustion end. Hence simulations or models, usually conducted at initial particle size, should be compared in terms of K rather than t_b. This strengthens the interest of K measurements through image processing. A corollary is that burning times deduced from K do not exactly match actual t_b measurements from PM. On average, we find that extrapolated burning times D_0^2/K are 13 % longer than measured.

3.2. Pure CO

As mentioned in the introduction, only Bucher et al. [9] considered combustion in pure CO—at atmospheric pressure only—and they reported a weak combustion driven by heterogeneous reactions. In this work, we have considered pure CO at higher pressures ranging between 1 and 15 atm. As depicted in Fig. 6, we clearly note, right after melting, the formation of different spots of condensed phase on the particle surface, appearing brighter in the images. Aluminum particle is then progressively fully covered and, at that point, luminous emission of the particle drops (not seen in Fig. 6). An envelope flame is not visible, at any time. Combustion therefore stops quite early, presumably due to the formation of a passivating layer around the particle. We here speak of "combustion" since particle is glowing—meaning that surface temperature is high—well after the laser has been stopped (signals not shown here). Tests conducted in inert gas (pure N_2) do not lead to such behavior, i.e. no bright spots on surface and light emission ceases right after laser removal. The absence of any diffusion flame is also confirmed at higher pressures (here, 15 atm). Yet, high pressures give a more intense light emission together with increased duration. Such effect of pressure supports a heterogeneous kinetically limited regime. Overall, those results are in line with Bucher et al. [9] and consistent with significant heterogeneous reactions between CO and aluminum surface. Aluminum in CO does not seem to react in the gas phase as the breakdown of the CO molecule requires a large quantity of energy compared to CO_2 for instance. As a last remark, the bright spots of condensed products forming on the surface do not clearly merge unlike in O_2 atmosphere. This would suggest for different non-miscible compounds, in agreement with different oxycarbides found by Rossi et al. [10]. Unfortunately, burnt out particles could not be collected and detailed *post-mortem* chemical analysis was not possible.

Figure 6: Typical combustion sequence in pure CO (p=3 atm, D_0=82 μm.)

3.3. CO_2/CO mixtures

CO_2 and CO are typical oxidizers released by solid propellant combustion so that their mixtures are highly relevant to aluminum combustion in solid rocket chambers. As already mentioned, a systematic study on CO_2/CO mixtures has not been reported so far. Results from the previous section suggest that aluminum can react with CO through surface reactions but does not burn in a diffusion flame. Our objective here is to assess whether CO has a synergistic or, on the contrary, inhibitive effect when aluminum burns with CO_2. Mixtures of CO_2/CO have therefore been studied at p=1 atm with CO molar fraction taken to 10-20-40-60 %.

Figure 7 presents the overall burning time t_b as a function of initial diameter D_0 for such mixtures. Note that for the highest CO fraction tested (60 %), combustion with a clear diffusion flame persists, although higher CO fractions were not investigated. Overall, increasing CO fraction leads to longer combustion times, confirming that CO has a much smaller oxidizing efficiency compared to CO_2. Burning times are found to scale as $t_b \propto D^n$ with n=1.7 ± 0.2 for such mixtures with lower n for CO-rich mixtures ($n \approx 1.5$ for CO=60 %). As for pure CO_2, Beckstead's correlation is found to lead to longer burning times, 21 % in average. The deviation is larger for high CO fractions and reaches 33 ± 8 % for the 60 % CO case.

Here again, direct image processing confirms a D^2

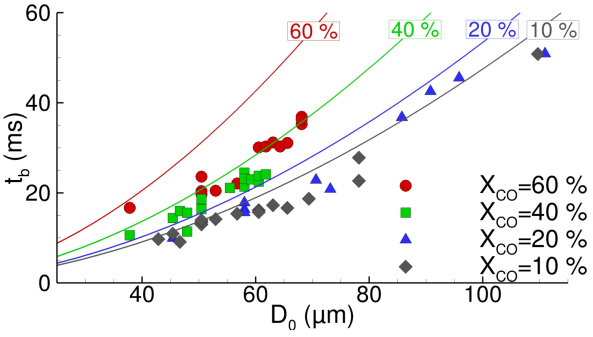

Figure 7: Burning time t_b as a function of initial diameter D_0 in CO_2/CO with different CO fractions (p=1 atm). Lines: Beckstead's correlation Eq. (1).

behavior in early combustion regimes. The resulting

evaporation constant K is plotted in Fig. 8. Because CO is not explicitly accounted for in Beckstead's correlation, we expect $K_{Beckstead} \propto X_{CO_2}$. Therefore, we have plotted K=$K_{CO_2}X_{CO_2}$ (with K_{CO_2}=296 μm^2/ms measured in pure CO_2) for comparison, and it is noted that this linear relationship correlates fairly well our results. But what would be theoretically expected if CO were purely inert regarding combustion ? Following usual D^2 theory for a droplet in a quiescent atmosphere, we expect $K \propto \ln(1+B)$ with the (thermal) Spalding number defined as B=$[c_p(T_\infty - T_s) + QY_{CO_2}]/L$ with c_p the aluminum heat capacity ($\approx$ 1100 J/kg/K), T_s the surface temperature (here, taken to 2700 K), L the aluminum latent heat of vaporization L=10.8 MJ/kg, and Q the aluminum heat of reaction per mass of CO_2 Q=11 MJ/kg [10]. The variation of K with CO_2 molar fraction X_{CO_2} then becomes

$$K = K_{CO_2}\frac{\ln(1+B)}{\ln(1+B_{CO_2})} \qquad (2)$$

which is plotted in Fig. 8 in dotted line. It seems that for CO-rich atmospheres, the measured K is roughly equal or even slightly lower than predicted by Eq. (2). This would call for an inert or weakly inhibitive behavior of CO. Considering combustion in pure CO, a possible mechanism for inhibition would be a reduction of available burning surface due to enhanced production of condensed species on the surface.

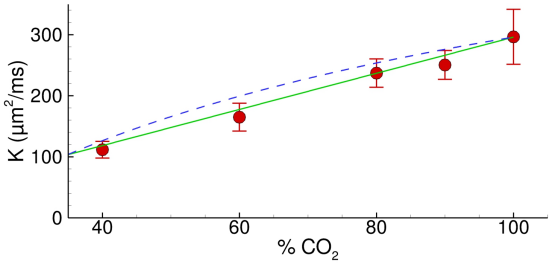

Figure 8: Evaporation constant K from direct imaging in CO_2/CO mixtures as a function of the molar CO_2 fraction (p=1 atm). Solid line: K=$296X_{CO2}$. Dotted line: theory with inert CO Eq. (2).

3.4. CO_2/N_2 mixtures

The same CO_2 mixtures were studied now replacing CO by a strong oxidizer (O_2) or a supposedly inert gas (N_2). Results, only presented in terms of K here, are compiled in Fig. 9 at pressure p=1 atm. The large increase of K with O_2 content is expected, confirming that O_2 is a stronger oxidizer than CO_2. The role of N_2 is similar to CO for high CO_2 fraction (say, above 80 %). For lower CO_2 fractions, some differences are

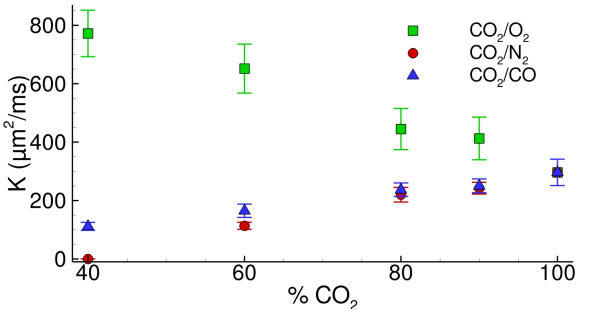

Figure 9: Evaporation constant K as a function of the molar CO_2 fraction mixed with CO, O_2 and N_2 (p=1 atm).

visible between N_2 and CO, with a lower combustion rate in N_2 mixtures, roughly by 30 %, for the 60 % CO_2 case. Interestingly, combustion is no longer possible for 60 % N_2 while it remains self-sustained for 60 % CO. Since thermal and mass diffusivities for CO and N_2 are almost identical, this means that this difference arises from a chemical effect, with either a slight oxidizing contribution of CO or, on the opposite, an inhibitive behavior of N_2. We do believe in the latter assumption with a passivating role of N_2 for some reasons. The first one is that we have already pinpointed in Fig. 8 that CO was—in the frame of the D^2 model—at most inert. Second, we have noticed some significant differences in the combustion between CO_2-N_2 and CO_2-CO, with an early transition to an asymmetric flame regime for N_2-rich mixtures. This effect was already confirmed by some of our previous experiments [7] in which combustion in O_2/N_2 and O_2/Ar differed qualitatively—although burning times were similar. Unlike O_2/Ar, combustion in O_2/N_2 led to a rapid and massive formation of oxide lobe and an early transition to asymmetric flame regimes with significant particle jetting and spinning, which was already noticed by Dreizin [20]. To some extent, this effect seems to persist here in CO_2/N_2 mixtures. The underlying physical mechanism for this effect of N_2 is unclear so far but one assumption, proposed by Dreizin [20], is related to the formation of NO in the flame. This species, which is also attested by simulations [21], could then diffuse back to the particle and react with aluminum through surface reactions creating oxides, nitrides or oxynitrides that further passivate the particle surface. In any case, our results support that N_2 and CO are not completely inert and should be accounted for in burning time correlations. Note that N_2 remains an abundant species in solid rocket motors, especially in future green propellants that incorporate nitrogen-rich molecules (e.g. azide-based polymers or

nitroamine molecules).

The expected mass fraction of NO species has been estimated from chemical equilibrium simulations. For the case 60 % CO_2/40 % N_2, NO fraction is about 1.1×10^{-5}, which is small due to the low predicted flame temperature (2690 K). For comparison, the same computation, replacing CO_2 by O_2, gives a NO mass fraction of 1.9×10^{-2} for a flame temperature of 3880 K. Note however that zero-dimensional chemical equilibium oversimplifies the complexity of the droplet combustion, so that direct numerical simulations with detailed kinetics are expected to have a more reliable estimation of NO formed in the flame.

3.5. A new burning time correlation

We propose here a new Beckstead-style empirical correlation for combustion times, but which should be more relevant for mixtures containing large amount of CO_2, CO or N_2. We have considered all the burning times obtained in this work (292 data points), with pressure ranging from 1 to 15 atm and diameters from 30 to 130 μm. A least square minimization is conducted using a Simplex algorithm, which yields the following "Beckstead-like" correlation

$$t_b = \frac{0.00213 D_0^{1.72}}{p^{0.12}[X_{O_2} + 0.18 X_{CO_2} + \mathcal{H}_{CO_2}.(0.03 X_{CO} - 0.01 X_{N_2})]} \quad (3)$$

The indicator function $\mathcal{H}_{CO_2}$ is 1 when CO_2 is the oxidizer and 0 otherwise. It is used to avoid non-physical finite burning time in pure N_2 or pure CO. Exponents for diameter (1.72) and pressure (0.12) are quite close to Beckstead (respectively, 1.8 and 0.1). However, the oxidizer efficiency for CO_2 is found slightly lower, 0.18 vs. 0.22. The efficiency for carbon monoxide is very low (0.03) while N_2 is basically inert (−0.01). All measurements are at ambient temperature so that temperature dependence is not available. If needed, it is still possible to include the Beckstead $T^{0.2}$ term.

The relevance of this new correlation is compared in Fig. 10 to our measured burning times for different CO_2-O_2-N_2-CO mixtures. Overall, this shows improvements compared to Beckstead's correlation (dashed lines) which overestimates burning times, at least for present mixtures and conditions. This is especially noticed for low CO_2 content.

We are aware that this correlation should include H_2O, which is a major oxidizer in solid rockets, before claiming for generality. This is one of our future works. In particular, the role of N_2 and CO with H_2O (which is considered as a stronger oxidizer than CO_2) is worth studying.

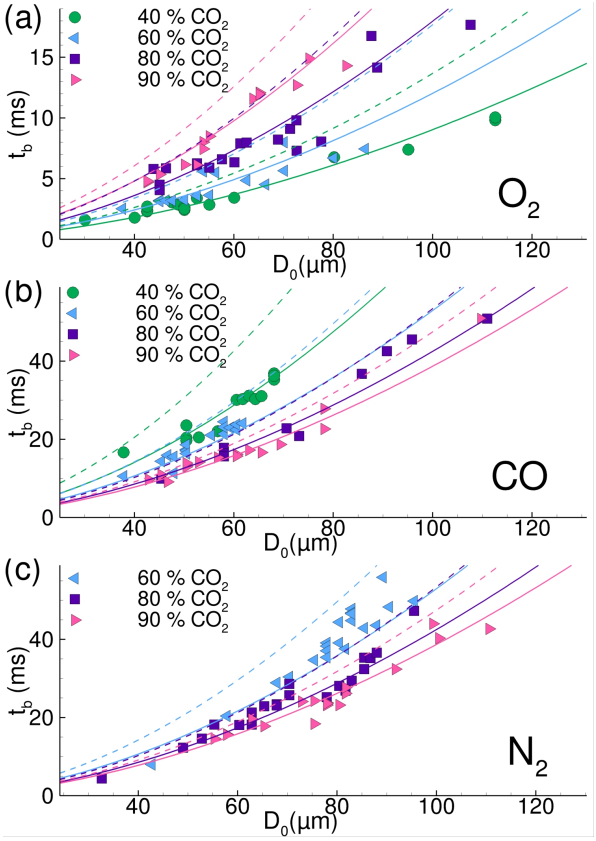

Figure 10: Measured and predicted burning times for aluminum burning in CO_2 mixed with O_2 (a), CO (b) and N_2 (c) (p=1 atm). Solid lines: new correlation Eq. (3). Dashed lines: Beckstead's correlation Eq. (1)

4. Conclusion

This paper considers aluminum combustion in CO_2-CO-N_2 mixtures using a recently developed experimental set-up which allows for high-frequency, high-resolution images of a single, levitated, burning aluminum particle. Aluminum is found to burn in pure CO_2 with a visible diffusion flame and we have reported burning time data scaling as $D_0^{1.9} p^{-0.1}$. In pure CO, we confirm that the particle undergoes a weak combustion as observed by Bucher et al. [9]. The oxidation is sustained by heterogeneous reactions, without any envelope flame. It quickly comes to a halt, supposedly due to the formation of a passivation layer on surface, and this behavior qualitatively persists at higher pressures (at least, 15 atm). Combustion in mixtures of CO_2 and CO

suggests an almost inert effect of CO. CO_2/N_2 mixtures similarly give ~~a~~ globally inert behavior of N_2. There are however slight differences between CO and N_2, when mixed with CO_2, with apparent slight inhibitive effect of N_2, in relation with possible enhanced formation of condensed species on particle surface which could be attributed to NO formation and subsequent reactions with aluminum. Processing some 300 burning time data eventually gives a new correlation which improves the widely-used Beckstead's correlation, at least in CO_2-CO-N_2 mixtures.

Future works will focus on the role of H_2O and mixtures thereof as well as direct numerical simulations with detailed kinetics to help understand present results. The role of H_2O is indeed crucial as it is abundant in solid propellant gases, is a stronger oxidizer than CO_2, and with very few experimental data. So far, the set-up has been modified to handle water vapor, notably a heating system and water vapor supply. Forthcoming experiments are expected to study mostly H_2O/CO_2 and H_2O/O_2 mixtures to estimate accurately the oxidizing efficiency of water.

Acknowledgments

This work was funded by the French Government Defense Procurement Agency DGA (*Direction Générale de l'Armement*).

References

[1] Y. Gan, L. Qiao, Combustion characteristics of fuel droplets with addition of nano and micron-sized aluminum particles, Combust. Flame 158 (2) (2011) 354–368.

[2] L. Soler, J. Macanás, M. Munoz, J. Casado, Aluminum and aluminum alloys as sources of hydrogen for fuel cell applications, J. Power Sources 169 (2007) 144–149.

[3] J. Bergthorson, S. Goroshin, M. Soo, P. Julien, J. Palecka, D. Frost, D. Jarvis, Direct combustion of recyclable metal fuels for zero-carbon heat and power, Appl. Energ. 160 (2015) 368–382.

[4] R. Lomba, P. Laboureur, C. Dumand, C. Chauveau, F. Halter, Determination of aluminum-air burning velocities using PIV and laser sheet tomography, Proc. Combust. Inst. 37 (2019) 3143–3150.

[5] A. Genot, S. Gallier, T. Schuller, Model for acoustic induced aluminum combustion fluctuations in solid rocket motors, J. Prop. Power 35 (4) (2019) 720–735.

[6] M. Beckstead, Correlating aluminum burning times, Combust. Explo. Shock Waves 41 (5) (2005) 533–546.

[7] A. Braconnier, C. Chauveau, F. Halter, S. Gallier, in: Eleventh Mediterranean Combustion Symposium (MCS-11), Tenerife, Spain, 2019.

[8] R. J. Gill, C. Badiola, E. L. Dreizin, Combustion times and emission profiles of micron-sized aluminum particles burning in different environments, Combust. Flame 157 (11) (2010) 2015–2023.

[9] P. Bucher, R. A. Yetter, F. Dryer, E. Vicenzi, T. Parr, D. Hanson-Parr, Condensed-phase species distributions about al particles reacting in various oxidizers, Combust. Flame 117 (1) (1999) 351–361.

[10] S. Rossi, E. L. Dreizin, C. K. Law, Combustion of aluminum particles in carbon dioxide, Combust. Sci. Technol. 164 (1) (2001) 209–237.

[11] T. Bazyn, H. Krier, N. Glumac, Oxidizer and pressure effects on the combustion of 10-micron aluminum particles, J. Prop. Power 21 (4) (2005) 577–582.

[12] J. Servaites, H. Krier, J. Melcher, R. Burton, Ignition and combustion of aluminum particles in shocked H_2O/O_2/Ar and CO_2/O_2/Ar mixtures, Combust. Flame 125 (1) (2001) 1040–1054.

[13] B. Legrand, M. Marion, C. Chauveau, I. Gokalp, E. Shafirovich, Ignition and combustion of levitated magnesium and aluminum particles in carbon dioxide, Combust. Sci. Technol. 165 (1) (2001) 151–174.

[14] A. Zenin, G. Kusnezov, V. Kolesnikov, in: 37th Aerospace Science Meeting and Exhibit, AIAA, 1999.

[15] A. Davis, Solid propellants: the combustion of particles of metal ingredients, Combust. Flame 7 (1963) 359–367.

[16] S. Turns, S. Wong, E. Ryba, Combustion of aluminum-based slurry agglomerates, Combust. Sci. Technol. 54 (1987) 299–318.

[17] A. Braconnier, C. Chauveau, F. Halter, S. Gallier, Detailed analysis of combustion process of a single aluminum particle in air using an improved experimental approach, Int. J. Energ. Mat. Chem. Prop. 17 (2) (2018) 111–124.

[18] A. Braconnier, S. Gallier, C. Chauveau, F. Halter, in: 37th International Symposium on Combustion, Poster 4P141.

[19] A. Braconnier, C. Chauveau, F. Halter, S. Gallier, in: 8th European Conference for Aeronautics and Space Sciences (EUCASS-2019), Madrid, Spain, 2019.

[20] E. L. Dreizin, On the mechanism of asymmetric aluminum particle combustion, Combust. Flame 117 (4) (1999) 841–850.

[21] M. Beckstead, Y. Liang, K. Pudduppakkam, Numerical simulation of single aluminum particle combustion, Combust. Explos. Shock 41 (2005) 622–638.